

Effect of rectangular damping groove on flow fluctuation and pressure pulsation for rotary energy recovery device through CFD simulation

Enle Xu^{a,b,c,*}, Xiaofeng Jiang^{a,c}, Zhenya Duan^a, Lefu Xie^b, Shichang Wang^c

^aCollege of Electromechanical Engineering, Qingdao University of Science and Technology, Qingdao 266061, China, email: xel360@126.com (E. Xu), jiangxf8822@163.com (X. Jiang), zyduan88@163.com (Z. Duan)

^bWeihai New Era Chemical Co., Ltd, Weihai 264200, China, email: xielefu1967@163.com (L. Xie)

^cSchool of Chemical Engineering and Technology, Tianjin University, Tianjin 300072, China, email: shi_chang001@126.com (S. Wang)

Received 11 September 2017; Accepted 3 April 2018

ABSTRACT

The rectangular damping groove was designed in the end plate aiming to control the flow fluctuation and pressure pulsation which is the inherent characteristic of RERD. The effect of the rectangular grooves on the transient pressure of the rotor duct and the flow fluctuation is investigated by the method of CFD simulation and theoretical analysis. The existence of the damping groove can prolong the time of the pressure change for the rotor duct. The flow fluctuation and pressure pulsation can effectively reduce from 23.04% to 2.95% and from 2.05% to 0.85%, respectively. According to the theoretical equation of the compressible liquid, a theoretical function was obtained involving the transient pressure of the rotor duct, the width and depth of damping groove, and the rotor speed. The simulative transient pressure of the rotor duct is in a good agreement with theoretical equation. Based on the simulation result, the lower rotor speed and pressure change in the rotor duct can soften the flow fluctuation and pressure pulsation, and the changing trend is in accordance with that of the previous experimental results, which indicating that the simulation model is reasonable. Based on the theoretical equation and simulation conclusion, an equation describes and quantifies the relation associated with the grooves and rotor speed. The research work can be applied to design an elegant rectangular damping groove to reduce the flow fluctuation and pressure pulsation.

Keywords: Rectangular damping groove; Flow fluctuation; Pressure pulsation; Rotary energy recovery device; Computational fluid dynamics

1. Introduction

The rotary energy recovery device (RERD) can effectively recover the pressure energy from the rejected high pressure brine based on the principle of positive displacement. RERD has become one of key facilities to save approximate 40% of the operating cost in the SWRO desalination [1–3], which is now a well-established water desalination way to solve the water shortage problem globally [4–7].

Fig. 1 represents the schematic of RERD. The device contains the high pressure (HP) zone, the low pressure (LP) zone and the sealed zone [8,9]. When the rotor ducts are in

the HP zone, the high pressure brine through the HP-IN of the brine end plate flow into the rotor ducts. The hydraulic energy of high pressure brine is transferred to the low pressure seawater in a direct momentary contact, and the pressurized seawater is discharged from the HP-OUT of the seawater end plate. When the rotor ducts are in the LP zone, the low pressure seawater through the LP-IN flows into the rotor ducts. The low pressure brine is pushed out through the LP-OUT. The sealed zone separates the HP zone and the LP zone [10–12].

When the rotor duct rotates from the LP zone to the HP zone, the high pressure stream runs into the rotor duct abruptly to increase the pressure instantaneously. When the rotor duct rotates from the HP zone to the LP zone, the high pressure stream of the rotor duct inflates into the low pressure

*Corresponding author.

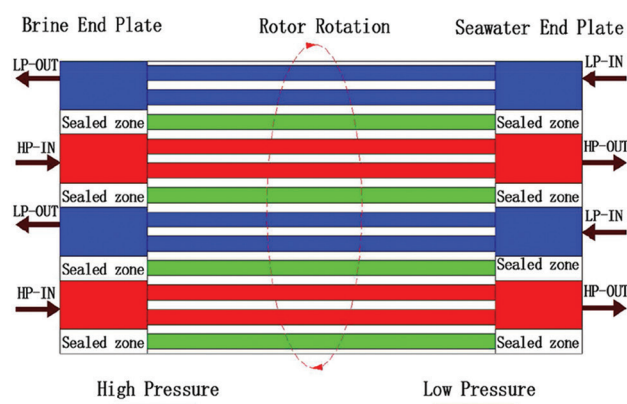


Fig. 1. Schematic representation of the RERD.

port abruptly to decrease the pressure instantaneously. So, with the rotor duct switching between HP zone and LP zone, the abrupt pressure change of the rotor duct will induce the flow fluctuation of the device which is the inherent characteristic of RERD [13,14]. Flow fluctuation results in pressure pulsation which is one of major sources on noise emission [15]. Noise level is one of important performance criteria except for the service life and efficiency for dynamic devices such as the RERD and the piston pump [16], thus it is necessary to study the characteristics of flow fluctuation and pressure pulsation.

Polizos et al. [17] pointed out that as the rotor ducts travel across the sealed zones, the alternating opening and closing of rotor ducts causes a considerable amount of noise. The damping groove formed in the sealed zones may have radial extensions, which is about 180° apart to balance the pressure between two zones of different pressure levels. The exact cross sectional shape, depth, and width of the groove show the relation with flow rates and the pressure of the device.

In order to run in a low noise level for the RERD, Bross et al. [18] provided a pressure-surge-reducing secondary flow zone at the transition between a housing-side inlet port and a housing-side sealed zone, and after flow zone at the transition between the end face openings of the rotor duct disposed in the rotor and the sealing webs of the rotor. Wang et al. [19] analyzed the effects of the pre-pressurization and pre-depressurization grooves on performance fluctuations of the RERD by means of CFD simulations and validating experiments.

Previous research revealed that the damping groove, formed in the end plate or the end face of the rotor, can reduce the flow fluctuation and the noise of the RERD. But the specific method and theory, how to design the dimension of the damping groove, was not yet given and mentioned.

This paper aims to design the rectangular damping groove in the end plate and diminish the flow fluctuation and pressure pulsation. Through CFD simulation, the effect of the rectangular grooves and the operational conditions on the transient pressure of the rotor duct and the flow fluctuation is investigated. Simultaneously, a theoretical formula is established to guide the design of an eligible damping groove for different RERD.

2. Theoretical and numerical methodologies

2.1. The design of the damping groove

The pre-pressurization damping groove exists where the LP rotor duct passes the sealed zone, while the depressurization damping groove exists where the HP rotor duct passes the sealed zone. This paper focuses on the four-port RERD, which have two HP and LP sealed zones, as well as two pre-pressurization and depressurization damping grooves. The pre-pressurization damping groove is used to increase the pressure of the rotor duct slowly, and the depressurization damping groove is to decrease the pressure of the rotor duct tardily. The pre-pressurization damping groove have the same structure and dimension with the depressurization damping groove, since the pressure variation is same for two kinds of damping grooves. The rectangular damping groove which is the simplest cross sectional shape was chosen in this paper.

Fig. 2 shows the end plate with the damping groove. The key parameters of damping groove are: the width of b , the depth of h , and the central angle of $\alpha_0 = 13.125^\circ$. The damping groove, connected with the forepart of the port, locates in the middle of the port. The rotor should pass the damping groove firstly, and then go into the port. Thus the rotor spins anticlockwise for the end plate.

2.2. Simulation model

The preprocessor ANSYS Workbench Design Modeler 14.5 was used as the geometry generator. Fig. 3 shows the three-dimensional geometric model of the simulation which was built based on Fig. 2. There are 12 circular rotor ducts with the height of 120 mm, and the rotor ducts distributed in the circle of 104 mm in diameter. One port covers just two rotor ducts. The clearance between the end plate and the rotor was so small to be ignored in order to simplify the computational model.

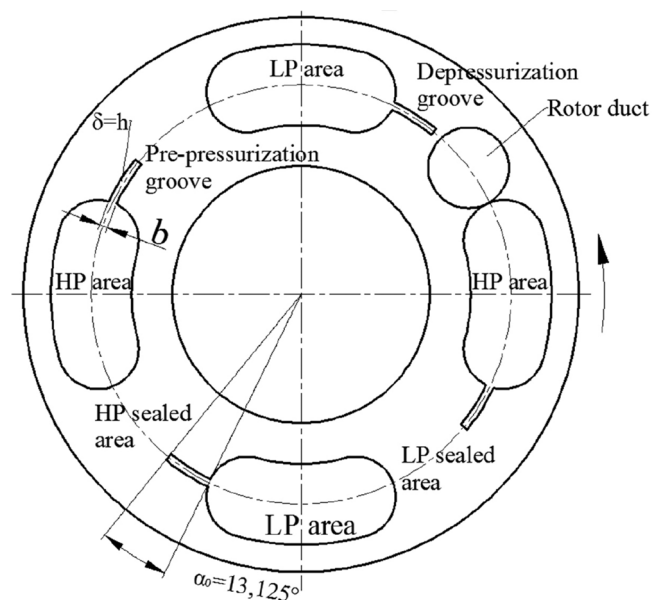


Fig. 2. The end plate with the damping groove.

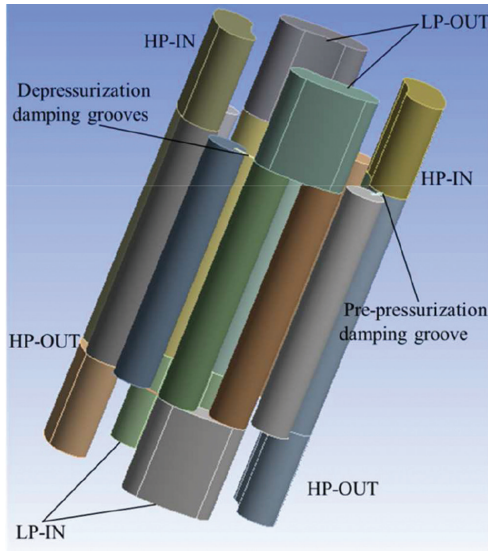


Fig. 3. Geometric model.

The computational grid of the model was made in the preprocessor ANSYS Workbench Meshing 14.5. The sweep method was used to generate grids for the model. Fig. 4 gives the grid model which contains 291535 cells, including hexahedral cells and mixed cells. Mesh dependency has been studied by examining different grid numbers. As no significant difference was found between the predicted results using more than 291535 cells, this grid number was used in the modeling to save computational time. The quality of the meshes was analyzed by using the orthogonal quality. The minimum orthogonal quality was 0.45, which indicated that the grids were nice [17].

2.3. Governing equations

The assumptions for the CFD model are as follows:

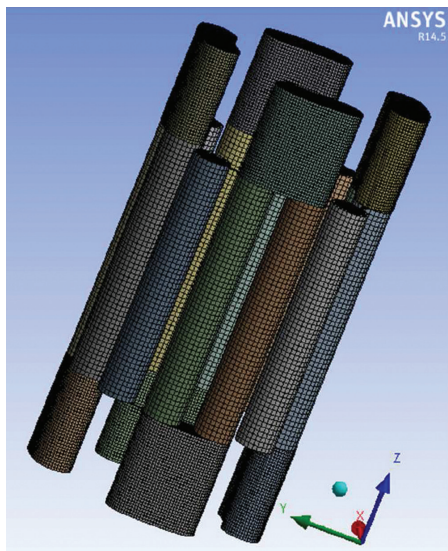


Fig. 4. Grid model.

1. The temperature of the seawater equals that of the brine, so no heat exchange involved in this process;
2. The viscous dissipation is negligible for this model.

The basic model equations based on the above assumptions are given in the following part. The continuity equation can be described as

$$\rho \nabla \cdot \vec{v} = 0 \quad (1)$$

where ρ is the density, and \vec{v} is the velocity vector.

The momentum equation is expressed as

$$\rho \frac{\partial \vec{v}}{\partial t} + \nabla \cdot (\rho \vec{v} \vec{v}) = -\nabla p + \nabla \cdot (\overline{\tau}) + \rho \vec{g} \quad (2)$$

where p is the static pressure, $\overline{\tau}$ is the stress tensor (described below), and $\rho \vec{g}$ is the gravitational body force.

The stress tensor is given by

$$\overline{\tau} = \mu (\nabla \vec{v} + \nabla \vec{v}^T) \quad (3)$$

where μ is the molecular viscosity.

The turbulent viscosity, μ_t , is calculated under the standard k - ϵ model where k is the turbulent kinetic energy and ϵ is the dissipation rate. The turbulent viscosity is computed by the following equation

$$\mu_t = \frac{c_\mu \rho k^2}{\epsilon} \quad (4)$$

The turbulent kinetic energy equation simplifies to

$$\frac{\partial(\rho k)}{\partial t} + \frac{\partial(\rho k u_i)}{\partial x_i} = \frac{\partial}{\partial x_j} \left[\left(\mu + \frac{\mu_t}{\sigma_k} \right) \frac{\partial k}{\partial x_j} \right] + G_k - \rho \epsilon \quad (5)$$

The turbulent dissipation ratio equation simplifies to

$$\frac{\partial(\rho \epsilon)}{\partial t} + \frac{\partial(\rho \epsilon u_i)}{\partial x_i} = \frac{\partial}{\partial x_j} \left[\left(\mu + \frac{\mu_t}{\sigma_\epsilon} \right) \frac{\partial \epsilon}{\partial x_j} \right] + \frac{c_1 \epsilon}{k} - c_2 \rho \frac{\epsilon^2}{k} \quad (6)$$

where u_i is the time mean velocity, G_k represents the generation of turbulence kinetic energy due to the mean velocity gradients. The model constants c_1 , c_2 , c_μ , σ_k , and σ_ϵ have the following default values: $c_1 = 1.44$, $c_2 = 1.92$, $c_\mu = 0.09$, $\sigma_k = 1.0$, $\sigma_\epsilon = 1.3$ [20].

2.4. Simulation scheme

The governing Eqs. (1)–(6) were solved using the commercial CFD software Fluent 14.5. The pressure-based solver was used to solve the governing equations. The PISO pressure-velocity coupling algorithm, standard pressure, first-order upwind discretization scheme turbulent for kinetic energy and dissipation energy were employed in the modeling. The second-order upwind discretization scheme was chosen in the moment equation.

The contact surfaces were used as the interface for transferring the data among the end plates, the damping

groove and the rotor ducts. The sliding mesh technique as a fully transient approach was used for the simulation of the rotor motion. For all the sliding mesh simulations, a time step equal to a cell was adopted in order to reduce the residual of the velocity and the continuity. The simulation could be treated as a convergence when the residual is below 0.001. One half time step was also tested, however practically identical results were found.

The water-liquid, regarded as the compressible flow with the bulk modulus of 2.2 GPa, was used in this simulation instead of the seawater and the brine. The reference density of this liquid is 998.2 kg/m³ with the density exponent of 7.15 at the reference pressure of 101325 Pa.

The boundary conditions for inlets and outlets are velocity-inlet and pressure-outlet, respectively. The velocity magnitude is determined as 1.132 m/s, and the velocity direction is normal to the boundary for the HP-IN and LOW-IN. The pressure of LP-OUT and HP-OUT is constant of 101325 Pa and 6.0 MPa, respectively. As regards the initial condition, all models were filled with the low pressure fluid.

The simulation convergence is assumed to be achieved when: (i) the flow rate of fluid entering and leaving the model are balanced; (ii) the averaged flow rate of the HP-IN reaches a stable level.

3. Results and discussion

3.1. The reason for flow fluctuation and pressure pulsation

The compressibility of the fluid will result in the volume change of the fluid when the pressure of the fluid uprushes or slumps, which are the main reason for flow fluctuation and pressure pulsation.

According to the theoretical equation of compressible liquid, Eq. (7), the varying volume of the fluid for one rotor duct can be calculated when rotor duct rotates from LP (HP) zone to HP (LP) zone. For this model, the varying volume is about to $1.01 \times 10^{-7} \text{ m}^3$.

$$\Delta p = -K \frac{\Delta v}{V} \quad (7)$$

where Δp is the changed pressure, Pa; K represents the bulk modulus of compressible liquid, Pa; V is the volume of one rotor duct, m³; Δv represents the varying volume, m³.

Fig. 5 provides the leakage rate through one depressurization damping groove, obtained from the Fluent software at groove width of 2 mm, groove depth of 0.15 mm, and rotor speed of 150 rpm. The moment confirms as the initial statistic time ($t = 0$) when the rotor duct begins to go into the damping groove, and the moment is defined as the final statistic time when the rotor duct begins to connect with the port. By integrating the curve in Fig. 5, the obtained covering area just represents the accumulative leakage rate through one depressurization damping groove. For this case, the leakage rate of one damping groove is $4.82 \times 10^{-8} \text{ m}^3$. Due to the rotor duct connected with two damping grooves, so the varying volume of the fluid for one rotor duct is about $9.64 \times 10^{-8} \text{ m}^3$.

The relative error is only 4.6% between the theoretical volume and the simulation result, indicating the simulation model is reasonable. In addition, the compressibility of

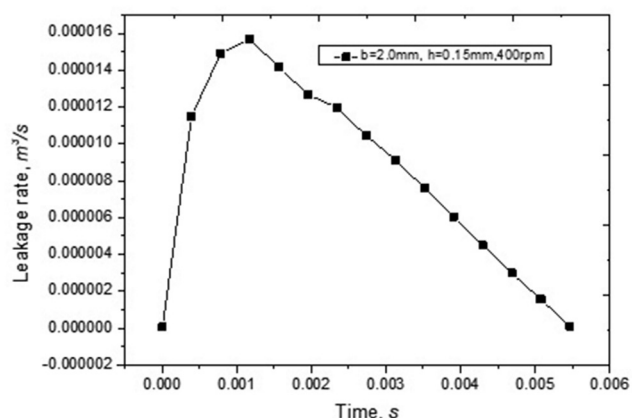


Fig. 5. The leakage rate through one depressurization damping groove.

the fluid cannot be neglected for the study of the flow fluctuation and pressure pulsation.

3.2. The reason for the existence of the damping groove

Fig. 6 gives the two-dimensional cutting plane with pressure contour at four different times. The cutting plane here used was expanded from a three-dimensional cylindrical surface with the diameter of 104 mm. The rotor duct moves from right to left. T_1 is the initial statistic time, and T_4 is the final statistic time, and T_2 and T_3 is the moment that the rotor duct connects with the damping groove at different position. In this figure, the red color refers to the high pressure, and the blue color represents the low pressure. From this figure, the pressure of the rotor duct increases or decreases slowly when the rotor duct moves in the LP or HP sealed zone.

Fig. 7 shows the transient pressure of the rotor duct for two models with or without damping groove when the rotor duct rotates from LP sealed zone to HP sealed zone. According to this figure, due to the existence of the damping groove, the pressure of the rotor duct changed gently in the sealed area compared to the counterpart without damping groove.

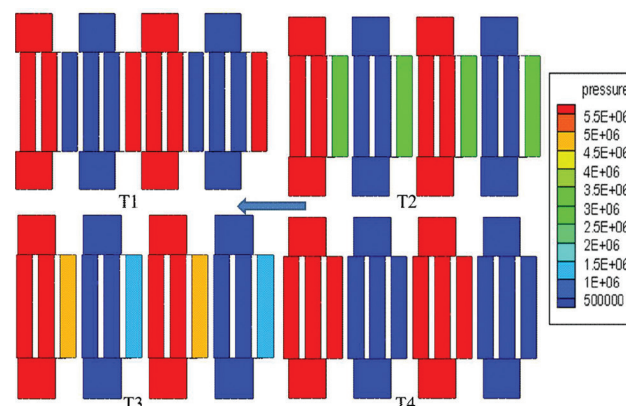


Fig. 6. The two-dimensional pressure contour of four different times.

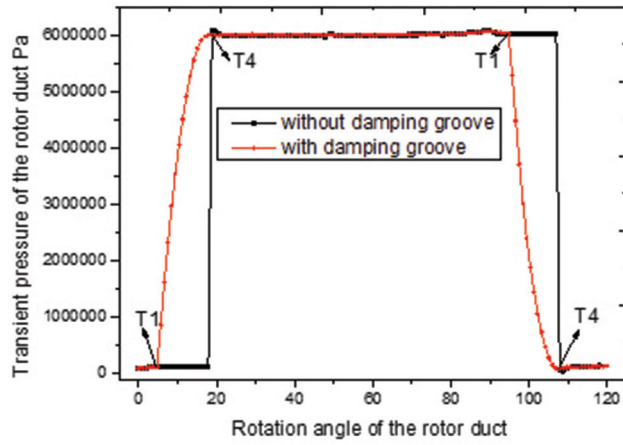


Fig. 7. The transient pressure of the rotor duct.

From two figures, it can be seen that the damping groove can prolong the changed time for the pressure of the rotor duct, which will lead to reduce the range of the flow fluctuation and pressure pulsation.

3.3. The theoretical transient pressure of the rotor duct

The depressurization damping groove can be regarded as the thin-walled hole. The leakage rate of the thin-walled hole can be calculated by the following equation:

$$Q = C_d A \sqrt{\frac{2}{\rho} \Delta P} \quad (8)$$

where Q is the leakage rate of the groove, m^3/s ; C_d is the contraction coefficient, 0.61–0.62 for the complete contraction, and 0.7–0.8 for the incomplete contraction; A is the sectional area of the damping groove, bh for this model, m^2 .

According to the characteristic of the device that one rotor duct connected with two damping groove in the sealed zone and Eq. (8), Eq. (7) can be redescribed as:

$$\frac{d\Delta p}{\sqrt{\Delta p}} = \frac{-2KC_d bh \sqrt{\frac{2}{\rho}}}{V} dt \quad (9)$$

where t is time that rotor duct rotate into the damping groove, s .

Using the initial conditions, the definite integral of Eq. (9) can be calculated by the following equation

$$\Delta p^{\frac{1}{2}} \Big|_{P_h - P_0}^{P - P_0} = \frac{-KC_d bh \sqrt{\frac{2}{\rho}}}{V_0} t_0^{30\alpha/\pi n} \quad (10)$$

where P is the transient pressure of the rotor duct, Pa; P_h is the pressure of the high pressure port, 6×10^6 Pa; P_0 is the pressure of the low pressure port, 101325 Pa; n is rotor

speed, rpm, α is the angle of rotor duct into the damping groove, rad.

The result of the definite integral can be expressed as

$$(P - P_0)^{\frac{1}{2}} - (P_h - P_0)^{\frac{1}{2}} = \frac{-30KC_d bh \sqrt{\frac{2}{\rho}}}{V_0} \frac{\alpha}{\pi n} \quad (11)$$

In order to simply Eq. (11), two new parameters, k and c , were defined as

$$k = \frac{-30KC_d bh \sqrt{\frac{2}{\rho}}}{V_0 \pi n} \quad (12)$$

$$c = (P_h - P_0)^{\frac{1}{2}} \quad (13)$$

So Eq. (11) can be simplified as

$$P = (c + k\alpha)^2 + P_0 = k^2\alpha^2 + 2kc\alpha + P_h \quad (14)$$

From Eq. (14), it is clear that there is a quadratic function relationship between the P and the α , and the P has the relation with b , h , and n .

3.4. Simulation transient pressure of the rotor duct

3.4.1. Relation between P and α

Fig. 8 shows the relation between P and α under different h , b and n . From Figs. 8a and b, it can be seen that at the same position of the damping groove, P decreases with the increment of h and b , since that results in bigger cross area to leak the fluid. From Fig. 8c it is clear that at the same position of the damping groove, P increase with the increment of the rotor speed, which takes less time to leak the fluid.

According to the fitting curve and the fitting equation in Fig. 8, the obtained quadratic fitting function between P and α correlates well with the simulation result since the correlation coefficient ($R^2 = 0.99$) is almost equal to 1, which is agreed well with Eq. (14). The simulative P_h is about to 6.0 MPa for different conditions, which is close to the practical pressure, indicating that Eq. (13) is reasonable.

3.4.2. Relation between k and h , b

Fig. 9a expresses the relation between k and h at $n = 400$ rpm, $b = 2.0$ mm, Fig. 9b shows the relation between k and b at $n = 400$ rpm, $h = 0.150$ mm. A linear relation between k and h , b could be found which is consistent with the trend of Eq. (12). In addition, for Fig. 9a, the relative error is 2.56% between the fitting slope of 7.21×10^6 and the theoretical slope of 7.03×10^7 which calculated according to Eq. (12). For Fig. 9b, the relative error is 5.12% between the fitting slope of 5.00×10^6 and the theoretical slope of 5.27×10^6 which calculated according to Eq. (12). Therefore, Eq. (12) is reasonable for different b and h according to the simulative results.

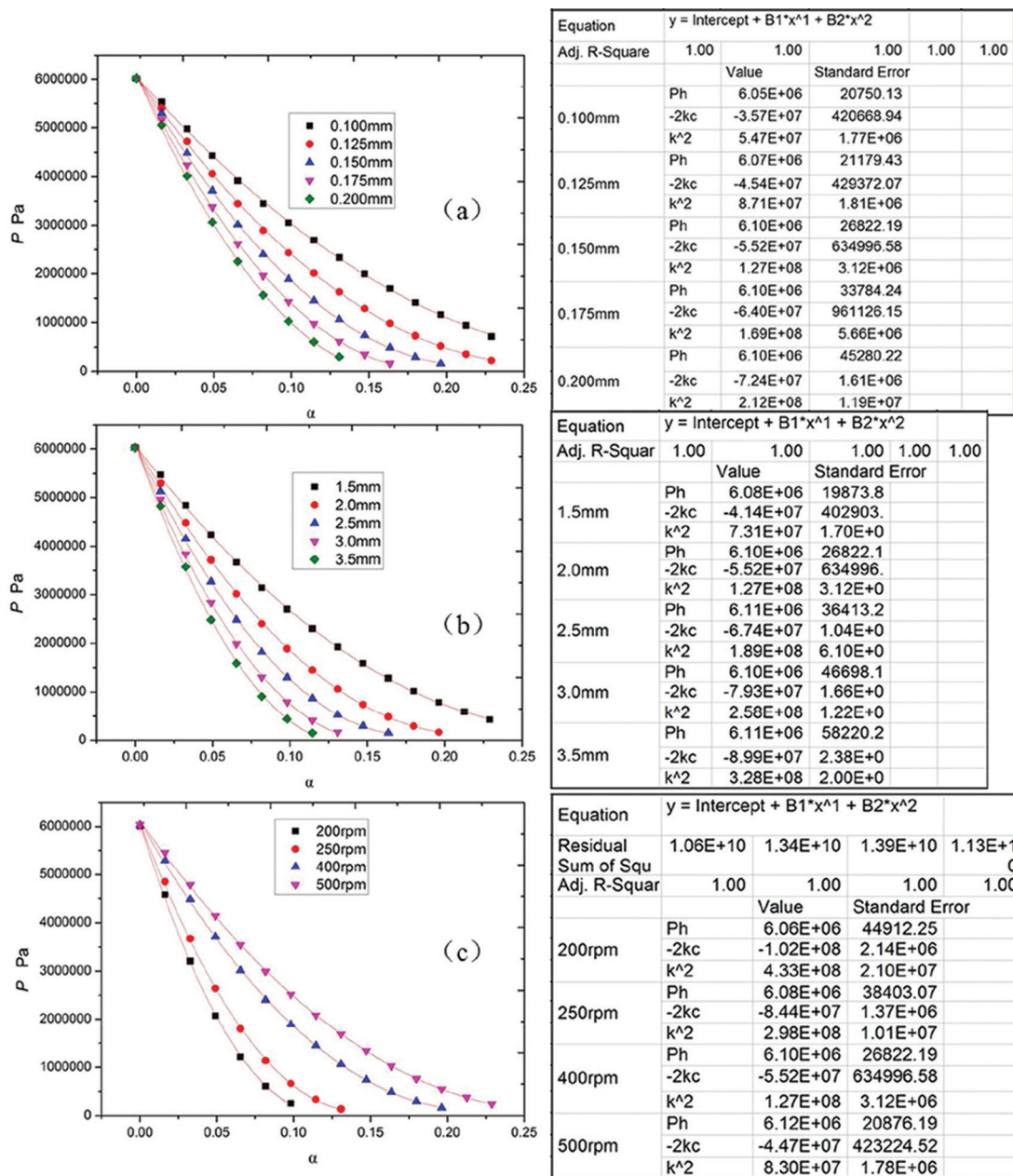


Fig. 8. Relation between P and α under (a) different h , $n = 400$ rpm, $b = 2.0$ mm; (b) different b , $n = 400$ rpm, $h = 0.150$ mm; (c) different n , $h = 0.150$ mm, $b = 2.0$ mm.

3.4.3. Relation between k and n

Fig. 10 expresses the relation between k and the reciprocal of rotor speed ($1/n$), at $b = 2.0$ mm, $h = 0.15$ mm. Similarly, a linear relationship was found between k and $1/n$ which is consistent with the trend of Eq. (12). In addition, the relative error is 7.13% between the fitting slope of 3.91×10^6 and the theoretical slope of 4.21×10^6 which calculated based on Eq. (12). Therefore, Eq. (12) is validated for different rotor speed.

In conclusion, the simulation results verified the relations between k and h , b , n , and between P and α under

different h , b , n , indicating that theoretical Eqs. (12)–(14) are very rational. Eqs. (12)–(14) can be used to calculate P instead of the method of simulation.

3.5. Effect on the flow fluctuation and pressure pulsation

Based on the theoretical and simulative models, this part aims to illustrate how the damping groove affects the flow fluctuation and pressure pulsation. The HP fluid was chosen as analytic target due to its negative effect on the reverse osmosis membrane.

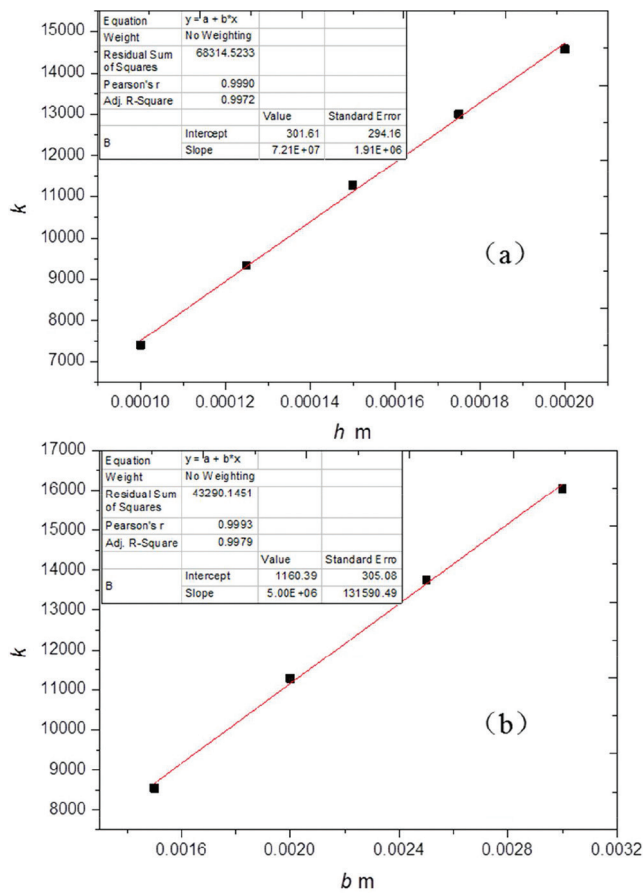


Fig. 9. Relation between k and (a) h under $n = 400$ rpm, $b = 2.0$ mm; (b) b under $n = 400$ rpm, $h = 0.150$ mm.

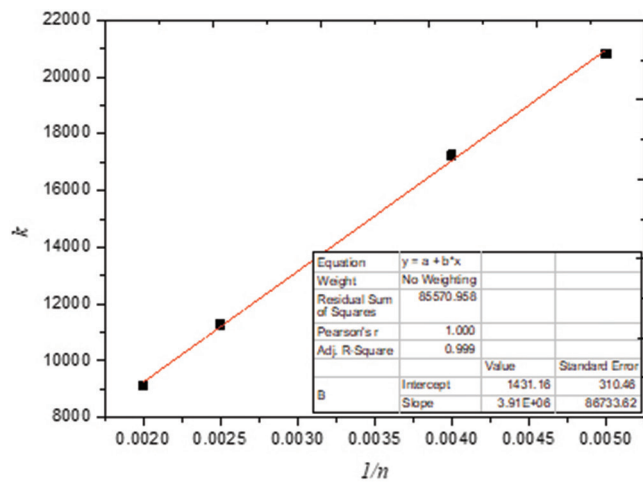


Fig. 10. Relation between k and $1/n$.

3.5.1. Effect of h and b on the flow fluctuation and pressure pulsation

Fig. 11 shows flow fluctuation and pressure pulsation under different h and b . In this figure, the triangles represent

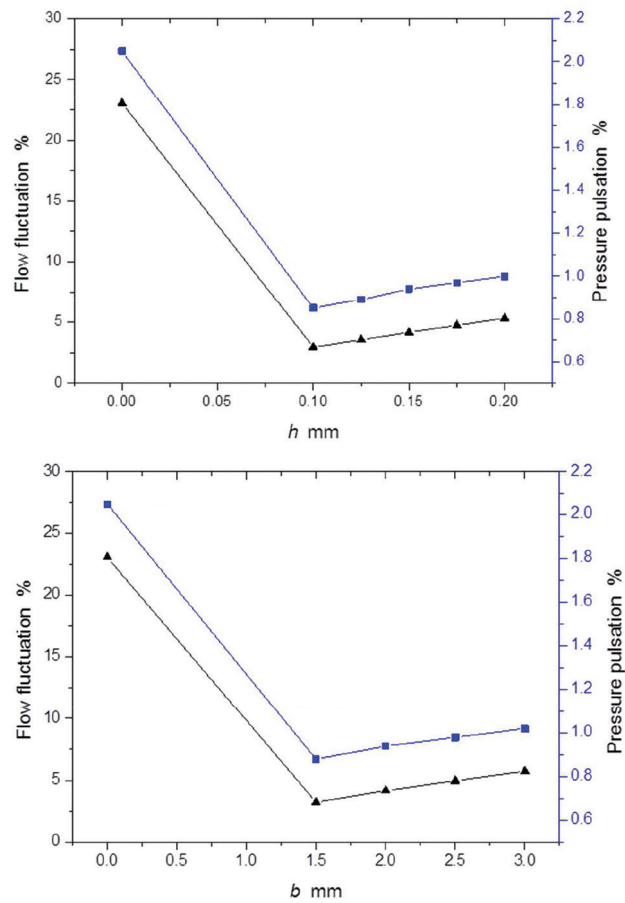


Fig. 11. Flow fluctuation and pressure pulsation under different h and b .

flow fluctuation, and the quadrangles stand for pressure pulsation. The flow fluctuation and pressure pulsation is the ratio between the variation and the average. The condition of $h = 0$ or $b = 0$ which is on behalf of the model without the damping groove, shows the maximal flow fluctuation of 23.0% and pressure pulsation of 2.05%.

From this figure, it is clear that the damping groove can effectively reduce flow fluctuation and pressure pulsation compared to the model without damping groove. The presence of damping groove can effectively reduce the flow fluctuation from 23.04% to 2.95% and pressure pulsation from 2.05% to 0.85%. In addition, the flow fluctuation and pressure pulsation decrease with the decrease of h and b . According to the slope of the fitting curve in Fig. 8, that is maybe because the pressure of the rotor duct changes slowly with the decrease of h and b .

3.5.2. Effect of n on the flow fluctuation and pressure pulsation

Fig. 12 provides the flow fluctuation and pressure pulsation under different n . From this figure, it can be found that flow fluctuation and pressure pulsation increase with the increase of n , and the changing trend is in accordance

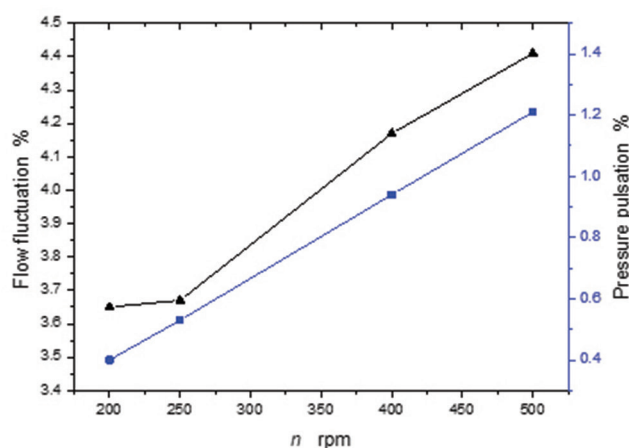


Fig. 12. Flow fluctuation and pressure pulsation under different n .

with that of the previous experimental results [19], indicating that the simulation model is reasonable.

In conclusion, the flow fluctuation and pressure pulsation decrease with the decrease of rotor speed and the slowness of the pressure change in rotor duct. The flow fluctuation and pressure pulsation is smallest when the pressure change is approximately linear in rotor duct. The mathematical expression is shown in Eq. (15). The maximal derivative of Eq. (14) with $\alpha = 0$ is equal to the slope of the pressure change in the linear trend.

$$P'_{max} = 2kc = \frac{p_h - p_0}{-\alpha_0} \quad (15)$$

According to Eqs. (12), (13), the Eq. (15) can be expressed

$$bh = \frac{V_0 \pi n (p_h - p_0)^{1/2}}{60 K C_d \alpha_0 \sqrt{\frac{2}{\rho}}} \quad (16)$$

From Eq. (16), there is some balancing limit between the rotor speed and grooves. The rotor speed is an important operational parameter for RERD. The minimum rotor speed can be determined according to the mixing and flow rate before the groove is designed. Eq. (16) shows the relation between groove and rotor speed which can guide the design of damping groove.

4. Conclusion

Flow fluctuation and pressure pulsation which is the inherent characteristic of RERD, results in the abrupt pressure change of rotor duct. In order to control flow fluctuation and pressure pulsation, the rectangular damping groove was designed in end plate, and the effect of damping groove on the flow fluctuation and pressure pulsation was investigated by the method of CFD simulation.

Based on simulation results, the liquid compressibility is the main reason for flow fluctuation and pressure

pulsation, and the existence of damping groove can prolong the time of pressure change in rotor duct. Compared to the model without damping groove, the damping groove can effectively reduce flow fluctuation from 23.04% to 2.95% and pressure pulsation from 2.05% to 0.85%.

According to the theoretical equation of compressible liquid and the damping groove regarded as thin-walled hole, a theoretical function was built among the transient pressure of rotor duct, the width and depth of damping groove, and rotor speed. The simulation results are in agreement with theoretical equation, indicating that the theoretical equation is reasonable. Based on the simulation results, flow fluctuation and pressure pulsation decrease with the slowness of the pressure change in rotor duct. The rise of rotor speed leads to the increase of flow fluctuation and pressure pulsation, and the changing trend is in accordance with that of the previous experimental results, indicating that the simulation model is reasonable. Based on the theoretical equation and simulation conclusion, an equation describes and quantifies the relation associated with the grooves and rotor speed. This research can be used to guide the design an elegant rectangular damping groove to reduce flow fluctuation and pressure pulsation.

Acknowledgments

This research is supported by Natural Science Foundation of Shandong Province (ZR2017BEE043), Science and Technology Program in Higher Education of Shandong (J17LC08) and Doctoral Fund of Qingdao university of Science and Technology (010022769).

References

- [1] D. Song, Y. Wang, S. Xu, Z. Wang, H. Liu, S. Wang, Control logic and strategy for emergency condition of piston type energy recovery device, *Desalination*, 348 (2014) 1–7.
- [2] E. Xu, Y. Wang, J. Zhou, S. Xu, S. Wang, Theoretical investigations on rotor speed of the self-driven rotary energy recovery device through CFD simulation, *Desalination*, 398 (2016) 189–197.
- [3] E. Xu, Y. Wang, J. Wu, S. Xu, Y. Wang, S. Wang, Investigations on the applicability of hydrostatic bearing technology in a rotary energy recovery device through CFD simulation and validating experiment, *Desalination*, 383 (2016) 60–67.
- [4] A. Zhu, P.D. Christofides, Y. Cohen, Effect of thermodynamic restriction on energy cost optimization of RO membrane water desalination, *Ind. Eng. Chem. Res.*, 48 (2008) 6010–6021.
- [5] A. Zhu, P.D. Christofides, Y. Cohen, Energy consumption optimization of reverse osmosis membrane water desalination subject to feed salinity fluctuation, *Ind. Eng. Chem. Res.*, 48 (2009) 9581–9589.
- [6] B. Qi, Y. Wang, S. Xu, Z. Wang, S. Wang, Operating energy consumption analysis of RO desalting system: Effect of membrane process and energy recovery device (ERD) performance variables, *Ind. Eng. Chem. Res.*, 51 (2012) 14135–14144.
- [7] L. Gao, A. Rahardianto, H. Gu, P.D. Christofides, Y. Cohen, Energy-optimal control of RO desalination, *Ind. Eng. Chem. Res.*, 53 (2014) 7409–7420.
- [8] I.B. Cameron, R.B. Clemente, SWRO with ERI's PX pressure exchanger device - A global survey, *Desalination*, 221 (2008) 136–142.
- [9] E. Xu, Y. Wang, L. Wu, S. Xu, Y. Wang, S. Wang, Computational fluid dynamics simulation of brine–Seawater mixing in a

- rotary energy recovery device, *Ind. Eng. Chem. Res.*, 53 (2014) 18304–18310.
- [10] R.L. Stover, A. Ameglio, P.A.K. Khan, The Ghalilah SWRO plant: An overview of the solutions adopted to minimize energy consumption, *Desalination*, 184 (2005) 217–221.
- [11] R.L. Stover, SWRO process simulator, *Desalination*, 221 (2008) 126–135.
- [12] S. Mambretti, E. Orsi, S. Gagliardi, R. Stover, Behavior of energy recovery devices in unsteady flow conditions and application in the modelling of the Hamma desalination plant, *Desalination*, 238 (2009) 233–245.
- [13] E. Mucchi, G. Dalpiaz, A. Rivola, Dynamic behavior of gear pumps: Effect of variations in operational and design parameters, *Meccanica*, 46 (2011) 1191–1212.
- [14] S. Kim, Y. Nam, M. Park, Design of port plate in gerotor pump for reduction of pressure pulsation, *J. Mech. Sci. Technol.*, 20 (2006) 1626–1637.
- [15] J. Kim, H. Kim, J. Jung, S. Oh, S. Jung, Relation between pressure variations and noise in axial type oil piston pumps, *KSME. Int. J.*, 18 (2004) 1019–1025.
- [16] J. Ma, Y. Fang, B. Xu, H. Yang, Optimization of cross angle based on the pumping dynamics model, *J. Zhejiang Univ-Sc. A.*, 11 (2010) 181–190.
- [17] T. Polizos, T. Babcock, L. Hauge, Pressure exchanger with an anti-cavitation pressure relief system in the end covers, U.S. Patent, 6540487B2, (2003).
- [18] S. Bross, W. Kochanowski, C. Schuler, Rotary pressure exchanger, U.S. Patent, 0104588, (2007).
- [19] Y. Wang, Y. Duan, J. Zhou, S. Xu, S. Wang, Introducing pre-pressurization/depressurization grooves to diminish flow fluctuations of a rotary energy recovery device: Numerical simulation and validating experiment, *Desalination*, 413 (2017) 1–9.
- [20] ANSYS Fluent User's Guide (release 14. 5) ANSYS, Inc: Canonsburg, PA, (2012).